Design of a Planar Solid State Transformer for DC Grids

Carolina da Costa Pinheiro de Avillez Pignatelli, Instituto Superior Técnico

Abstract

This project presents a high-frequency low-voltage (HFLV) planar modular solid-state transformer (SST) with a ferrite core and an 8 layers printed circuit board (PCB) with an improved partially half-turn interleaving winding structure.

The proposed transformer core was compared with different core geometries and materials. And, the proposed transformer winding structure was compared with other winding structures, taking into account leakage inductance and DC resistance.

The planar modular transformer with the proposed core and winding structure was simulated with finite element analysis software and tested in the laboratory. The transformer has a primary voltage of 400 V, a secondary voltage of 150 V, a switching frequency of 100 kHz, and, due to the winding structure modularity, the apparent power can vary from $S = 2,\ 4,\ 6\ kVA$, considering that each winding structure was designed to support 2 kVA. The efficiency of the transformer for nominal power of 2 kVA is around 95%. And, the efficiency of the transformer for nominal power of 4 kVA is around 97%.

Keywords: ferrite core; finite element analysis; high-frequency low-voltage; improved partially half turn interleaving winding structure; planar modular solid-state transformer; printed circuit board.

1. Introduction

Due to the exponential growth of renewable energies, electrical systems are rapidly evolving and new challenges are arising. It is now possible to generate power locally with renewable energy sources and integrate local storage. Also, with the advances in solid-state power electronics technology, hybrid systems using Alternating Current (AC) for the utility grid and Direct Current (DC) within infrastructures are now possible. The centralized generating facilities give way to smaller distributed generation facilities, meaning that the power production and distribution may involve microgrids. Microgrids are integrated energy systems that interconnect loads and distributed energy sources and can be operated connected to the grid or in island mode [1]. The main advantages of microgrids are: the easy integration of distributed micro-generators; the reduction of losses in the transmission and distribution system since generators and loads are closer to each other; the possibility to feed the loads with energy storage systems when there is an interruption in generation or a demand peak; and, the possibility to power local loads directly with a DC bus [2].

A microgrid consists of several distributed energy resource units and loads. It is possible to control and manage the power flow by using power electronic converters that interconnect power generation and energy storage in the grid[1] [3]. Smart grids are based on this Intelligent Energy Management (IEM) systems, allowing traditional energy sources to work hand in hand with renewable energy sources, and, thus, allowing bidirectional power flow, local controls, and management and monitoring capacity in the distribution systems.

Traditional AC microgrids are easy to be relieved at peak demand times or in the event of failure, as there is always a backup power supply that can be connected to the distribution system. However, as renewable energy sources are usually the main power supply of microgrids, the conversion stages of DC-DC-AC for connecting DC renewable energy sources and energy storage systems will decrease the overall system's efficiency [4].

In a DC microgrid the unnecessary DC-AC conversion is eliminated. A DC-AC converter is used as an interface with the power grid, resulting in improved system efficiency [5]. However, the voltage level used in microgrids may be considerably lower than that used in distribution systems, specially when used to connect low power loads, meaning that both AC and DC microgrids require a transformer to reduce the voltage level of the distribution system [6].

Traditional line frequency transformers (LFT) have simple construction, high efficiency and high reliability. Nonetheless, despite the robustness of the conventional transformer with an operating frequency of 50/60 Hz, it also has some disadvantages since this transformer is merely passive and does not meet the demands of smart grids. By decentralizing power generation with the integration of distributed renewable energy sources, distributed generation sources, and distributed energy storage devices, LFT are unable to deal with issues such as: voltage deregulation under-load or in no-load conditions, resulting in high losses (since the optimal performance of LFT is near the full-load) [7]; lack of power quality regu-

lation and control of active and reactive power flow that is necessary for the IEM flow in microgrids) [8]; harmonic distortion, reflection of input voltage sags, dips or frequency variations on the output (disturbances of the primary circuit are reflected in the secondary circuit) [9]. Also, due to the low operating frequency, the conventional transformer is a large, heavy, and bulky equipment [3] [5].

Hence, the main motivation of this document is the improvement and implementation of a new type of transformer - a planar solid-state transformer (SST) with high frequency of operation that can be used in microgrids. Therefore, the design and testing of a high-frequency low-voltage (HFLV) planar SST will be carried out.

2. State of the Art

2.1. Solid State Transformer in Smart Grids

In 1968, McMurray proposed an isolated converter that allowed high and medium frequency transformers to provide galvanic isolation by operating the switches at a higher frequency than the electric grid (with an operating frequency of 50/60 Hz) [10].

This association, known as Solid State Transformers (SST), Power Electronic Transformers or Intelligent Transformers, is considered key to replacing the conventional LFT in applications such as smart grids, where SST technology can facilitate the integration of renewable energy sources and storage systems with both DC and AC interfaces, being a powerful tool in the active energy management of microgrids. Hence, the IEM module can be an SST with intelligent power management and advanced communication capabilities [6].

SST are considered of great importance in applications where volume and weight restrictions apply. By increasing the operating frequency of the transformer, it is possible to reduce its volume and weight without increasing the winding current density or the maximum core flux density, as can be seen by the area product equation 1 and 2 [11]. Hence, by increasing the operating frequency, SST allows higher utilization of the magnetic core and reduction in the transformer size, resulting in a power density improvement [4].

$$A_p = \frac{P_t}{K_f K_u f A_c B_{max} J} \tag{1}$$

$$Volume \propto A_p^{\frac{3}{4}} \propto \frac{1}{f^{\frac{3}{4}}} \tag{2}$$

In which A_p is the core power handling, P_t is the total apparent power, K_f is the waveform coefficient, K_u represents the window utilization factor, f is the operating frequency, A_c is the core cross-section area, B_{max} is the maximum flux density, and J is the current density.

Unlike LFT, SST allow power flow control with a reactive power compensation feature that adjusts its input and output voltages and currents. This means that, with IEM, bidirectional energy flow control capability is now a possibility. Hence, this type of transformer can protect loads from power system disturbances and, the other way around, offering galvanic insulation and power quality enhancements [3]. SST facilitate compensation of voltage sags, provide short circuit protection by limiting the fault current, and allow for power factor correction due to the input current phase control [2].

The schematics of an LFT and an SST are presented in Figure 1. Note that SST also have the possibility of providing a DC voltage. This DC bus and the DC-DC converter provide isolation since the input and output voltages are now decoupled [2]. Also, by allowing the interface of DC and AC, it makes it possible to facilitate the power flow between microgrids, as it provides output voltage regulation [4]. In Figure 2 the architecture of a microgrid based on an SST is presented.

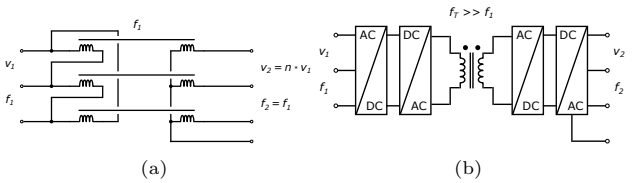

Figure 1: (a) Typical delta-wye-connected LFT configuration vs. (b) SST configuration in a distribution grid application.

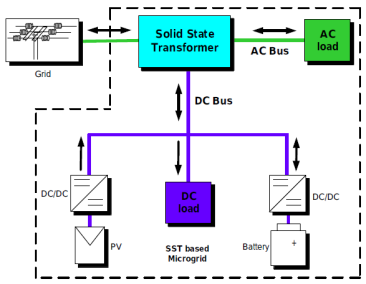

Figure 2: SST-based microgrid architecture. Adapted from [2].

Another characteristic of most SST topologies is the modular and expandable structure. With this feature, SST achieve high reliability due to redundant converter cells. This is an essential attribute in applications where SST can replace LFT, as in distribution grid applications, since each module design is optimized and optimal combination of different modules can be achieved. Also, modular structures have reduced design, manufacturing and maintenance cost due to the design standardisation.[4].

In conclusion, SST are considered the solution for specific applications, such as the future smart distribution grids and applications with weight and volume constraints, due to the desirable characteristics of high power density, fault tolerance, and modularity. Also, the extra degrees of freedom that SST provides can result in a more robust electrical network due to its high ability to adapt to changes in

operation, voltage and frequency regulation and the ease of accommodating energy storage.

Despite these advantages, the implementation of SST in the distribution grid has some challenges. The cost of an SST is higher than that of an LFT since the control circuitry is expensive. Still, an effective cost reduction can happen associated with the mass production of SST for several applications and the advances in semiconductor technology, namely in the category of Wide Bandgap semiconductors. In addition, the required standard efficiency for a distribution transformer must be higher than 97%, and, nowadays, SST's overall system efficiency is lower than 97%. Also, LFT are very reliable and require little maintenance. However, SST have a high number of semiconductors, which increases the possibility of failure and makes them less reliable. Another concern is the compatibility and implementation of SST in the distribution grid, as the entire power system was developed for LFT. Hence, the grid infrastructure must change to lodge SST requirements and achieve a smart grid. Changing the whole grid is unrealistic and has a very high cost, so SST must start by being implemented in micro and nanogrids [12].

In spite of the disadvantages referred above, there are applications where the most important characteristic is neither directly the efficiency nor the cost of the solution. An example of this is the aerospace and space industries where power density must be maximized, otherwise in the long run the additional weight and volume may result in increased operation costs and energy consumption. Another example is in the charging infrastructure of electric vehicles, where despite the higher cost of SST, it allows increased power density which may result in increased number of charging spots. Finally, the flexibility introduced by intelligent transformers in microgrids and smart grids may revolutionize the way electricity is produced, transported, distributed and stored which may result in the decrease of the overall system operation costs, by allowing energy sources optimization and increased reliability.

2.2. Planar Solid State Transformer Characteristics

One of the current objectives in power electronics is to increase the power density of converters because their magnetic components occupy an essential volume and may limit the power electronic converter integration. Thus, by increasing the frequency of operation, using wide band gap semiconductors (as Silicon Carbide or Gallium Nitride) [13], the volume of power converters is reduced, and the power density increases [14].

Due to the eddy currents effect, conventional wire-wound magnetic components structure winding loss increases with high frequency, significantly above 100 kHz [15]. On the other hand, planar magnetics components are low-profile structures that use low-thickness copper strips windings. This means that the influence of skin and proximity effects is reduced, which allows these components to work at a higher frequency and have a higher power density than conventional magnetics [16]. Hence, planar magnetics for high-frequency power conversion are a competitive and effective approach to downsizing, an essential feature in high power density converters.

The major advantages of planar magnetics are:

- Low profile - Due to their low profile, planar cores are different from conventional cores made with helical windings. By reducing the height of the winding window, planar cores have a higher effective area for the given effective volume. Therefore, planar magnetics use flat windings made of printed circuit board (PCB) tracks or copper foils, which allows for a shorter winding area [15].

- Enhanced thermal performance - Due to the lower profile of the planar core, there is a larger cross-sectional and surface areas to volume ratio, providing more contact area to the heat exchange surface, which facilitates the removal of heat from the planar magnetic component. Thus, the thermal resistance of planar cores is lower when compared to conventional cores [17] [18].

- Easy to manufacture, low cost, and excellent repeatability - Unlike conventional winding design, in which the wire sizes and shapes are limited, planar winding design can be adapted to the sizes and shapes of the individual turns. PCBs windings are easily integrated into mass production due to their excellent repeatability, enabled by the winding structure, which reduces costs [15].

- Controlled leakage inductance - PCBs allow the interconnection of arbitrary layers, making the interleaving of primary and secondary windings implementation much easier than with conventional magnetics. This results in a reduction in high-frequency winding losses and in a controlled leakage inductance [19]. Leakage inductance can also be reduced by minimizing the number of turns, reducing the total winding area.

- Modularity - PCBs for planar windings allow passive components, like semiconductors, to be assembled on the PCB. Thus, no extra connections are required, and the space used is optimized.

Although planar magnetics offer several advantages, it also has some limitations:

- Large footprint area - Due to the large surface area of the planar core, if the core window is fully utilized, the windings will extend outward of the core and be exposed, increasing the footprint of the planar magnetic component [15]. It is possible to reduce the footprint if the PCB windings are hidden inside the core. However, this means that the core cross-section will be reduced.

- Low copper fill factor and window area - Safety standards, like Institute of Printed Circuits (IPC) design specification IPC-2221 [20], dictate the minimum distances between windings and limit the copper fill factor. In addition, with PCB windings, a higher portion of the winding window is filled with a dielectric material, reducing the window utilization factor [17].
- Limited number of turns - Planar core's high cross-section area combined with low copper fill factor results in a limited number of turns for PCB winding. Also, to increase the number of turns, it is necessary to reduce the winding width, which increases the ohmic resistance of the conductor (DC resistance), or have a higher number of layers, which is not a cost-effective solution.
- High winding stray capacitance - Although PCBs reduce the leakage inductance by placing the windings closer together, it results in an unwanted effect of increased parasitic capacitance due to limited clearance and creepage distances. This gives rise to high capacitive coupling between the windings [21]. By increasing the insulation between the winding layers, which results in higher isolation, it is possible to reduce stray capacitances with the downside of increasing leakage inductance.

2.3. Planar Core Geometry

The most common planar core types are EE or EI core. These cores were specifically designed for planar magnetics and have a rectangular center leg. Therefore, they require a longer turn that extends beyond the core, giving rise to possible electromagnetic interference (EMI) and higher space usage.

There are other planar cores that are low-profile versions of standard cores like RM, ER, PQ, etc. These cores have a circular center leg, thus, they have lower mean length turn, MLT, and better EMI shielding. However, these cores have a smaller winding window area to core area ratio than the E core, limiting the number of winding turns [17].

Having a lower number of turns or a lower mean length turn results in lower winding loss and leakage inductance, as shown in equations (3) and (4). However, in planar transformers applications with medium and high current, a smaller winding area means a higher winding resistance, which results in higher power loss. Hence, the rectangular center leg core has a lower winding loss (DC resistance) than the rounded center leg core. Therefore, since the AC resistance increases at higher frequencies due to the increase of proximity and skin effects, the rounded center leg core has higher eddy current losses in the windings. As the skin effect increases, the temperature in the windings also increases, resulting in more significant power losses. Because the winding area of rectangular center leg cores is higher than in circular center leg cores, EE and EI cores are less sensitive to winding losses [22], and their current density converts less energy into heat [23].

$$R_{trace} = \rho \frac{MLT}{A_{w_{cu}}} \left[1 + \alpha (T_{temp} - T_{amb})\right] \tag{3}$$

$$R_{cu} = N R_{trace} \tag{4}$$

R_{trace} represents the copper trace resistance, MLT is the copper mean length turn, the copper winding area A_w is the trace thickness T times the trace width W, $\alpha = 3.9 \times 10^{-}3\ \Omega/^{\circ}C$ is the copper temperature coefficient, T_{temp} is the temperature of operation of the copper strip, and $T_{amb} = 25\ ^{\circ}C$ is the ambient temperature.

2.4. Planar Core Material

The selection of core materials is one of the most important steps in the transformer design. The proper core material selection can reduce core losses, and this choice depends on the frequency of operation. Some of the most relevant requirements for choosing the core material are [11]: saturation magnetic flux density, relative permeability, core loss density, and operating temperature characteristics.

The major groups of transformer core materials available on the market are: iron alloys, amorphous materials, powder core materials, and soft magnetic ferrites [11].

In iron alloys, silicon steel is the most used magnetic material. It has high saturation flux density at low frequencies and good permeability at high flux density. However, at higher frequencies, its losses increase drastically.

Amorphous materials as 2714A have the advantage that high-frequency applications present high resistivity, high permeability, high saturation magnetic flux density, and low core losses.

Nanocrystalline materials have low core losses, high saturation flux density, and are stable at high temperatures. When comparing amorphous materials and nanocrystalline materials, although amorphous materials have higher core losses than nanocrystalline materials, nanocrystalline have a higher cost.

Iron powder is the typically used powder core material. It has very low permeability and very high losses at high frequency.

Soft ferrites can be divided into manganese-zinc (Mn-Zn) and nickel-zinc (Ni-Zn). These materials present high resistivity, high permeability, low conductivity, and low core losses at high frequencies. However, they have a small saturation magnetic flux density and are unstable at high temperatures. Typically Mn-Zn is used at frequencies lower than 2 MHz and Ni-Zn at frequencies between 1 MHZ to hundreds of MHz.

The usual core material in conventional transformers is silicon steel. However, this material is only suitable at low frequency due to its increasing losses at high frequency. The most common core materials at high frequency are amorphous alloys, nanocrystalline, and soft magnetic ferrite materials [24]. To choose the best core material for

each application, a trade-off between volume, cost, thermal management, efficiency (power loss) and power density must be done.

2.5. Planar Windings

At high frequency, the skin and proximity effect are very high and the winding losses become the most significant losses of the planar transformer [25]. Therefore, the main requirement in planar windings is to minimize the winding's AC resistance.

A study using different winding types was performed in [26] to reduce skin and proximity effect. In this study, four types of winding configurations with the same footprint and dimension were compared, taking into account the AC resistance, and skin and proximity resistances. The results obtained demonstrate that the AC resistance increases with a higher number of turns and frequency. Also, at a lower frequency the skin resistance is the predominant aspect of AC resistance, and it decreases with the increase of the cross-section area of the conductor. However, the proximity effect increases at higher frequencies and controls the AC resistance. Using a solid winding with reduced track width improves the proximity resistance compared with the solid winding with maximum allowable track width.

Also, a comparison of the AC to DC resistance ratio in solid coils with different track widths was performed in [27]. The AC to DC resistance ratio increases for a higher number of winding turns for constant track width. And by adjusting the track width, it is possible to change the AC to DC resistance ratio while using a higher number of turns in the windings.

3. Planar Core Characteristics

3.1. Application and System Requirements

In this thesis, a planar modular transformer that ensures galvanic isolation and bidirectional power flow will be designed. This planar transformer can be used to connect an energy storage system to a nanogrid. The nanogrid layout can be as presented in Figure 3.

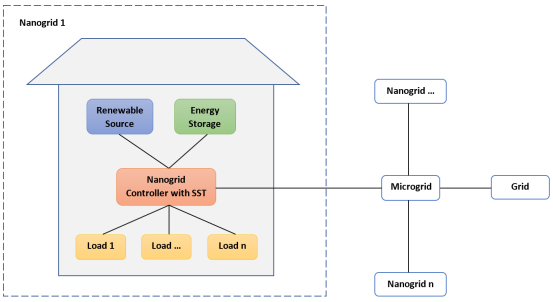

Figure 3: Nanogrid block diagram.

Figure 4 shows the application system that will be used in this project. At the input, it was considered that there will be $V_{DC} = 400\ V$ modulated by a converter connected to a planar single phase modular transformer with primary voltage $V_{prim} = V_{DC} = 400\ V$. It was also considered that the planar transformer apparent power is 6 kVA. The transformer windings will be sized to support $S = 2\ kVA$. It is thus possible to test the transformer for 2, 4, and 6 kVA by connecting the windings in parallel. The cost of mass production of flat windings is relatively cheap and easy to manufacture, which is a crucial advantage of this topology. For example, if a module of windings fails, it is possible to easily replace it. Also, with this type of structure, it is possible to manufacture identical windings to ensure different levels of power or voltage according to the application requirements.

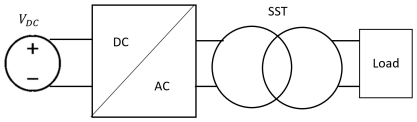

Figure 4: Application system.

The system will feed a battery of approximately $V_{bat} \approx 110\ V$ at 100% capacity (two batteries of 48 V in series). The planar core properties must be known to determine the number of primary and secondary turns.

3.2. Core choice

To choose the core material and geometry, it was necessary to consider the geometries and materials that the leading manufacturers of planar core transformers have available as standard models. Since there is no planar core transformer made of amorphous material available in the market, and soft ferrite materials are the most used in this industry, a ferrite core was chosen. Also, ferrites are extremely cheap when compared to materials belonging to the amorphous and nanocrystalline material classes.

After reaching out to Magnetics Inc., which has one of the broadest lines of standard ferrite materials, this company provided us the core used for this application. Magnetics Inc. also presents an extensive core loss modeling, which provide more accurate results when computing the core losses. The main objective is to have a core with high permeability, high flux density, and low losses at 100 kHz. According to Magnetics Inc., for power transformer planar cores ferrite applications, the preferred materials are: F, L, P, R and T [28].

According to Magnetics Inc. catalogue, the only planar ferrite core that can support 6 kVA is the model 49938. The transformer core will be made of ferrite R material, whose properties are in Figure 5.

3.3. Core Losses

Ferrite Core Loss Calculator from Magnetics Inc. was used to calculate the ferrite material core loss at various frequencies and temperatures [30]. The core loss is given by equation (4.7).

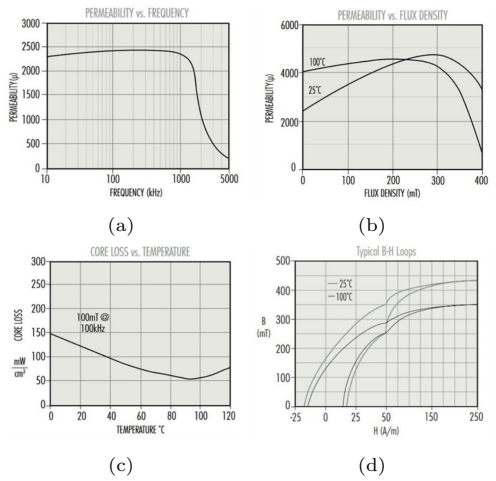

Figure 5: R material properties: **a)** Permeability *vs.* Frequency. **b)** Permeability *vs.* Flux Density. **d)** Core Loss *vs.* Temperature. **e)** Typical B-H Loop. Adapted from [29].

$$P_c = \frac{a f^x B^y L(T)}{1000} \tag{5}$$

Where,

- P_c is the core loss (mW/cm^3);
- f is the frequency of operation (Hz);
- B is the peak flux density (T);
- T is the temperature $(°C)$;
- $L(T) = \begin{cases} b - c(T) + d(T)^2, & \text{if } T \neq 100\ °C \\ 1, & \text{if } T = 100\ °C \end{cases}$;
- the a, x, y, b, c, d parameters change according to the ferrite material and the frequency range.

The final core losses are given by equation 6, where $V = 79.8\ cm^3$ is the core volume.

$$P_c = P[mW/cm^3]V[cm^3] \tag{6}$$

3.4. Planar Core Design Equations

It is now possible to calculate the required turns for the transformer's primary, N_{prim}, and secondary windings, N_{sec}.

$$N = \frac{V}{K_f f A_c B_{max}} \tag{7}$$

$K_f = 4$ represents the waveform coefficient for a square wave, $A_c = 540\ mm^2$ is the cross-section area of the core, and $B_{max} = 250\ mT$ is the maximum flux density. Hence, $N_{prim} = 8$ turns, and $N_{sec} = 3$ turns. Therefore, the transformer turns ratio is $n = \frac{8}{3}$.

The specifications for the High-Frequency Low-Voltage (HFLV) planar transformer are listed in Table 1.

Table 1: Specifications of the HFLV planar modular transformer.

Nominal Power Rating per Module S	$2\ kVA$
Nominal Power Rating S	$6\ kVA$
Voltage Rating V_{prim}/V_{sec}	$400\ /\ 150\ V$
Switching Frequency f	$100\ kHz$

4. Planar Winding Characteristics

4.1. Leakage Inductance

Leakage inductance causes the input current to vary at a low rate between zero and the rated value, $\frac{di(t)}{dt}$. Also, leakage inductance results in stored energy outside of the core that leads to generation of voltage spikes, creates EMI problems and increases switching losses [31]. Therefore, for this project, the windings must be designed to ensure that leakage inductance is as small as possible.

To decide the winding arrangement for the PCB, leakage inductance was calculated by analyzing the MMF and energy distribution of the planar transformer.

$$W_{stored} = \frac{1}{2}\int_{total} BH\, dV = \frac{1}{2} L_l I^2 \tag{8}$$

A partially interleaving half-turn structure was analyzed, as seen in Figure 6. It as a MMF distribution of 10 $A.turn$, and the middle layers sustain half the current by putting two layers in parallel. Furthermore, the winding loss will decrease since the copper width in the parallel layers increases. Therefore, the windings for this application will be an 8 layers PCB with a partially interleaving half-turn structure 2P-S-2P-S*-S*-2P-S-2P.

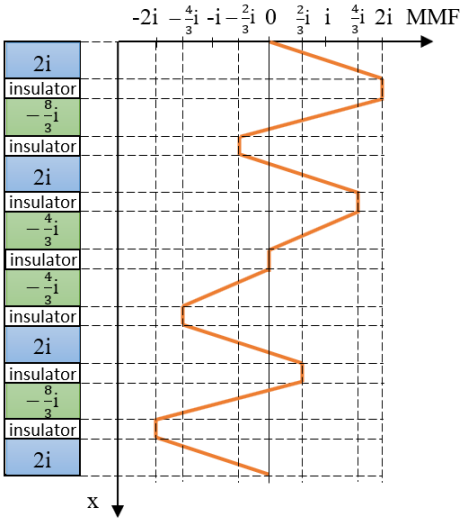

Figure 6: Analytical MMF distribution for partially interleaving half turn 2P-S-2P-S*-S*-2P-S-2P structure.

4.2. PCB Design and Copper Losses

It is possible to compute the winding loss for the minimum widths and spacing used in the PCB, as can be seen in Table 2.

Table 2: Winding loss for the first version of the PCB.

	W_{coil} $[mm]$	$s_{coil\ to\ coil}$ $[mm]$	R_w $[m\Omega]$	P_w $[W]$	$P_{w_{total}}$ $[W]$
Primary (2 coils*4 layers)	4	3	233.54	5.84	12.36
Secondary (1 coil*2 layers)	15		15.57	5.15	
Secondary Parallel (1 coil*2 layers in parallel)	7		16.68	1.38	

By using the minimum widths and spacing there is space in the PCB that is not being used, which means that the coils' width can be increased. Therefore, lower copper losses can be achieved. The final PCB layout with lower copper loss can be seen in Figure 7

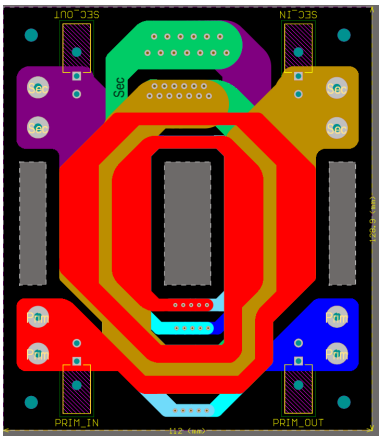

Figure 7: Final PCB layout from Altium Designer software.

5. Finite Element Modeling and Analysis

5.1. Simulation Setup

In order to have a more reliable simulation in Ansys software, the air gap between the two parts of the core must be calculated. To do so, an open-circuit test was performed in the Laboratory. First, the secondary winding was open-circuited to measure the primary winding self inductance with a LCR Meter. The same process was performed for the secondary winding. The self inductances measured in the laboratory are shown in Table 3. To reduce the air gap it was applied pressure in the core, which is reflected in the results by increasing the self inductances.

Table 3: Self inductances measured in the laboratory with a LCR Meter for $T_{amb} \approx 25$ °C at 100 kHz.

	Self inductance without pressure in the core $[\mu H]$	Self inductance with pressure in the core $[\mu H]$
$N_{prim} = 8$	$L_{prim} = 451$	$L_{prim} = 572$
$N_{sec} = 3$	$L_{sec} = 64$	$L_{sec} = 80$

5.2. PCB Simulation

A Magnetostatic Optimetrics analysis - an automatic variational analysis - was performed to understand the variation of self inductance for different air gaps. According to Figure 8, the self inductances measured in the laboratory $L_{prim} = 572\ \mu H$ and $L_{sec} = 80\ \mu H$ are obtained for an air gap of approximately $l_g \approx 33\ \mu m$.

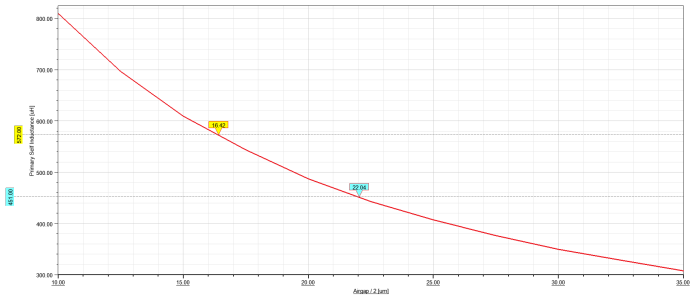

Figure 8: Self inductance sweep for a range of air gap on the primary winding.

Now that the core material properties and the air gap are defined in the simulation, it is possible to compute the magnetization current, I_{mag}, in a Transient analysis in conjunctio with Simplorer: $I_{mag} \approx 2\ A$, as seen in Figure 9.

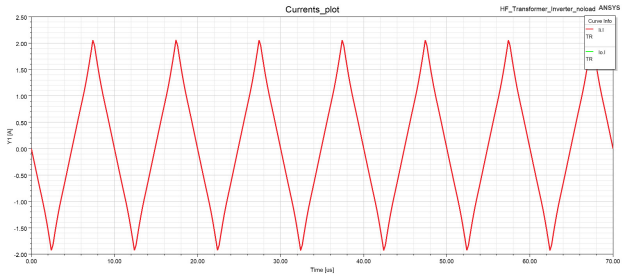

Figure 9: Primary winding magnetizing current from Ansys co-simulation from Ansys Maxwell 2D and Ansys Simplorer.

The primary winding was excited with $I_{mag} = 2\ A$ in Ansys Magnetostatic. The inductances from Ansys Magnetostatic analysis are given in Table 4.

Table 4: Simulated inductances with $I_{mag} = 2\ A$ and $l_g = 33\ \mu m$ in Ansys Maxwell Magnetostatic analysis.

	Self inductance L $[\mu H]$	Mutual inductance L_M $[\mu H]$	Inductive Coupling Coefficient k
Primary	560.91	210.07	0.99846
Secondary	78.92		

Table 5 shows the leakage inductance obtained in Ansys Maxwell Magnetostatic simulation.

Table 5: Leakage inductances for 2P-S-2P-S*-S*-2P-S-2P partially half turn interleaving winding structure from Ansys Maxwell Magnetostatic analysis.

	Leakage inductance $[\mu H]$
$L_{l_{prim}}$	1.52
$L_{l_{sec}}$	0.20

In Figure 10 it is possible to observe the maximum core loss for 100 kHz is $P_c = 42.83\ W$, and the average core loss per period is $P_c \approx 21.42\ W$.

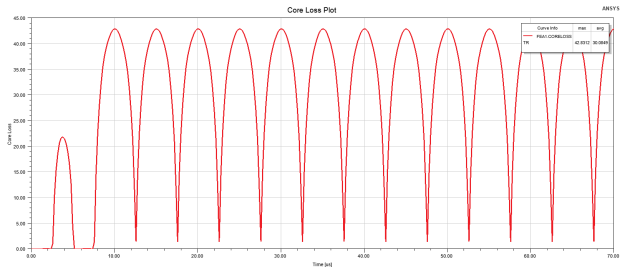

Figure 10: Core losses from Ansys co-simulation from Ansys Maxwell 2D and Ansys Simplorer.

6. Experimental Results

The next step was to test the transformer. The schematic of the laboratory setup and the final laboratory setup with the components that were used is shown in Figure 11.

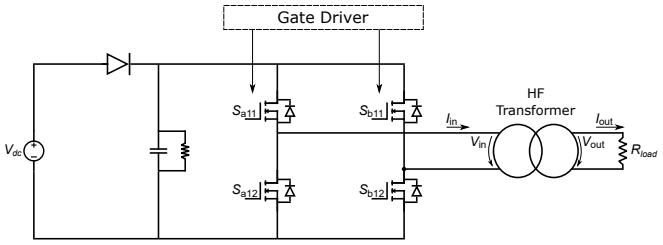

Figure 11: Laboratory system setup schematic.

6.1. Open-circuit Test for $f = 20\ kHz$

Despite showing the results for $f = 20\ kHz$, the objective is to understand how the transformer behaves at nominal conditions. Therefore, if at $f = 100\ kHz$ the primary voltage is $V_{prim} = 400\ V$ and the secondary voltage is $V_{sec} = 150\ V$, at $f = 20\ kHz$:

$$V_{p_{(f=20\ kHz)}} = \frac{20\ kHz\ V_{p_{(f=100\ kHz)}}}{100\ kHz} = 80\ V \tag{9}$$

$$V_{s_{(f=20\ kHz)}} = \frac{20\ kHz\ V_{s_{(f=100\ kHz)}}}{100\ kHz} = 30\ V \tag{10}$$

With rated voltage on the primary winding and with secondary winding open-circuited, the magnetizing current flows in the primary winding. This means that the peak magnetizing current obtained in the laboratory was $I_{mag_{laboratory}} = 1.48\ A$.

It is now possible to obtain the experimental B-H curve:

$$B(t) = \frac{\int \left(v_{prim}(t) - R_{prim} i_{prim}(t)\right) dt}{N_p A_c} \tag{11}$$

$$H(t) = \frac{N_{prim} i_{prim}(t)}{l_m} \tag{12}$$

With the obtained B-H curve in Figure 12, we demonstrate that the transformer does not saturate, and that the hysteresis curve is similar to the theoretical B-H curve given by Magnetics Inc.

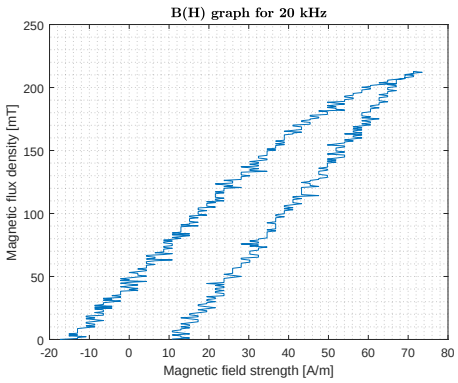

Figure 12: B-H curve obtained experimentally.

Also, from the B-H curve area it is possible to compute the average core loss per period.

$$P_c = 100\ kHz \times A_c l_m \int H\, dB \tag{13}$$

A comparison between the simulated and experimental average core loss per period is shown in Table 6.

Table 6: Simulated *vs.* experimental average core loss per period for $f = 100\ kHz$.

Simulated P_c $[W]$	Experimental P_c $[W]$	Error (%)
21.42	24.40	13.91

Lastly, the primary self inductance, L_{prim}, can be calculate using equation 14.

$$L_{prim} = \frac{V_{prim}}{\left(\frac{di_{prim}(t)}{dt}\right)} \tag{14}$$

Hence, $L_{prim} = 719.94\ \mu H$ for $f = 20\ kHz$. For $f = 100\ kHz$:

$$L_{prim_{(f=100\ kHz)}} = L_{prim_{(f=20\ kHz)}} \frac{\mu_{100\ kHz}}{\mu_{20\ kHz}} = 751.24\ \ \mu H \tag{15}$$

In Table 7 it is possible to compare the results obtained in the simulation and the laboratory.

Table 7: Simulated *vs.* experimental primary self inductances for $f = 100\ kHz$.

Simulated $L_{prim_{(f=100\ kHz)}}$ $[\mu H]$	Experimental $L_{prim_{(f=100\ kHz)}}$ $[\mu H]$	Error (%)
560.91	751.24	33.9

6.2. Short-circuit Test for $f = 20\ kHz$

The primary leakage inductance, $L_{l_{prim}}$, can be calculated using equation 16.

$$L_{l_{prim}} = \frac{V_{prim}}{\left(\frac{di_{prim}(t)}{dt}\right)} \tag{16}$$

Hence, $L_{l_{prim}} = 1.57\ \mu H$. In Table 8 it is possible to compare the results obtained in the simulation and the laboratory.

Table 8: Simulated *vs.* experimental primary leakage inductances.

Simulated $L_{l_{prim}}$ $[\mu H]$	Experimental $L_{l_{prim}}$ $[\mu H]$	Error (%)
1.52	1.57	3.29

6.3. Different Load Conditions Test

The last step was to analyze the efficiency of the transformer. First, different loads were used to see how the transformer behaves under rated power and near nominal power ($S = 2\ kVA$) for $f = 100\ kHz$. Since:

$$P_{out} = \frac{V_{prim}^2}{R_{load}} \tag{17}$$

for $R_{load} = [80, 100, 150, 200]\ \Omega$, the output power will be $P_{out} = [2, 1.6, 1.07, 0.8]\ kW$, respectively.

Finally, two PCBs were connected in parallel to measure the efficiency of the transformer with modular winding structures. Thus, different loads were used to see how the transformer behaves under rated power and near nominal power ($S = 4\ kVA$) for $f = 100\ kHz$. Therefore, for $R_{load} = [50, 60, 80, 100, 150, 200]\ \Omega$, $P_{out} = [3.2, 2.67, 2, 1.6, 1.07, 0.8]\ kW$, respectively.

In Figure 13 it is possible to observe the transformer efficiency at $f = 100\ kHz$ for $S = 2\ kVA$ and $S = 4\ kVA$. According to the results, the efficiency is higher for two PCBs in parallel ($S = 4\ kVA$) than for only one PCB ($S = 2\ kVA$),as it would be expected because the copper area is larger and the copper loss decreases while the core losses should remain approximately constant.

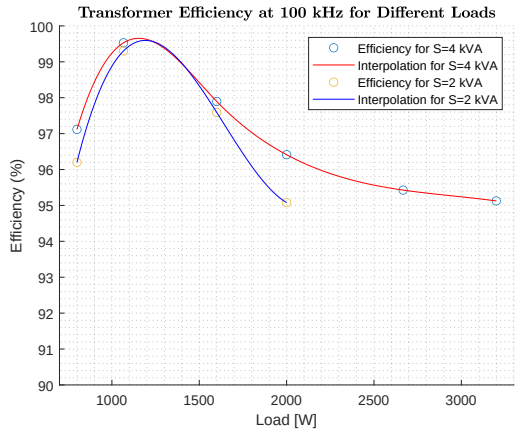

Figure 13: Comparison between transformer efficiency at $f = 100\ kHz$ for $S = 2\ kVA$ and $S = 4\ kVA$, obtained in the laboratory.

7. Conclusions and Future Work

7.1. Conclusions

In this project, a planar modular HFLV transformer with $f = 100\ kHz$, $S = 6\ kVA$ (where each PCB winding is design to work with $S = 2\ kVA$), $Vprim = 400\ V$ and $Vsec = 150\ V$ was designed.

After an in-depth study of all the characteristics that have a major impact on the choice of the planar core, such as the application specifications, the core geometry, core material, core specific material, and core air gap, a planar core from Magnetics Inc. was chosen. The geometry of the core is of type EE, since this is the only shape that is available for a power range of 6 kVA. The goal was to have an ungapped core because air gap increases core losses. Since the most suitable material for the planar core is ferrite, the ferrite R material was chosen due to its low core losses when comparing with other ferrite materials, specially at the frequency of operation of 100 kHz. Hence, the chosen core model was the 49938EE core from Magnetics Inc.

Then, the MMF distribution was analyzed for different winding structures and it was concluded that the leakage inductance would be smaller for the partially interleaving half turn 2P-S-2P-S*-S*-2P-S-2P winding structure with 8 layers. This winding structure also presents the smallest copper losses for the different winding structures that were analyzed. After, the PCB windings were designed for minimum and maximum copper width and spacing between the copper traces. Since, the copper losses are reduced by widening the runways as much as possible, the final PCB was designed with the maximum possible copper width.

A FEA simulation was performed with Ansys software, and it corroborated the theoretical results that were obtain regarding core losses and B-H curve. The accuracy of the achieved FEA model simulations from Ansys software was validated in the experimental open-circuit and short-circuit tests, since the obtained magnetizing currents, magnetizing inductances, leakage inductances, B-H curve and core losses are similar to the simulation values. The simulation results obtained for a load test with $P_{out} = 2\ kW$ at $f = 100\ kHz$ were also corroborated with the experimental results.

Finally, the efficiency of the transformer for nominal power of 2 kVA is around 95%. And, the efficiency of the transformer for nominal power of 4 kVA is around 97% in no load condition. This means that the modularity of the transformer windings can increase the transformer efficiency by placing PCBs in parallel.

7.2. Future Work

The modular transformer has an maximum apparent power of 6 kVA. Therefore, the next step would be to test the transformer efficiency with three PCBs in parallel, and, to test the transformer efficiency for $S = 2,\ 4,\ 6\ kVA$ with a higher number of loads to have a more detailed and reliable efficiency curve.

Since ringing interferes with the measured values and the calculated efficiencies, by studying the transformer losses and efficiency based on the thermal model of the transformer (with a calorimeter), the results obtained would be more accurate. Also, with the transformer ther-

mal study it is possible to analyze the maximum power of the transformer.

Finally, it would be interesting to study the behavior of the transformer efficiency if the input converter and the transformer were designed and integrated in a PCB. It is expected that the leakage inductance decreases, as well as the overall system efficiency, since the converter losses need to be taken into account.

References

[1] R. H. Lasseter. Smart distribution: Coupled microgrids. *Proceedings of the IEEE*, 99(6):1074–1082, 2011. doi: 10.1109/JPROC.2011.2114630.

[2] W. A. Rodrigues, L. M. F. Morais, T. R. Oliveira, R. A. S. Santana, A. P. L. Cota, and W. W. A. G. Silva. Analysis of solid state transformer based microgrid system. In *2016 12th IEEE International Conference on Industry Applications (INDUSCON)*, pages 1–6, 2016. doi: 10.1109/INDUSCON.2016.7874543.

[3] B. Viktor, I. Roasto, and L. Tõnu. Intelligent transformer: Possibilities and challenges. *Scientific Journal of Riga Technical University. Power and Electrical Engineering*, 29:95–100, 01 2011. doi: 10.2478/v10144-011-0016-8.

[4] J. E. Huber and J. W. Kolar. Solid-state transformers: On the origins and evolution of key concepts. *IEEE Industrial Electronics Magazine*, 10(3):19–28, 2016. doi: 10.1109/MIE.2016.2588878.

[5] X. She, A. Q. Huang, S. Lukic, and M. E. Baran. On integration of solid-state transformer with zonal dc microgrid. *IEEE Transactions on Smart Grid*, 3(2):975–985, 2012. doi: 10.1109/TSG.2012.2187317.

[6] X. She, S. Lukic, A. Q. Huang, S. Bhattacharya, and M. Baran. Performance evaluation of solid state transformer based microgrid in freedm systems. In *2011 Twenty-Sixth Annual IEEE Applied Power Electronics Conference and Exposition (APEC)*, pages 182–188, 2011. doi: 10.1109/APEC.2011.5744594.

[7] P. Barker and R. De Mello. Determining the impact of distributed generation on power systems. i. radial distribution systems. In *2000 Power Engineering Society Summer Meeting (Cat. No.00CH37134)*, volume 3, pages 1645–1656 vol. 3, 2000. doi: 10.1109/PESS.2000.868775.

[8] S. Ansari, A. Chandel, and M. Tariq. A comprehensive review on power converters control and control strategies of ac/dc microgrid. *IEEE Access*, 9:17998–18015, 2021. doi: 10.1109/ACCESS.2020.3020035.

[9] A. Elmoudi, M. Lehtonen, and H. Nordman. Effect of harmonics on transformers loss of life. In *Conference Record of the 2006 IEEE International Symposium on Electrical Insulation*, pages 408–411, 2006. doi: 10.1109/ELINSL.2006.1665344.

[10] W. McMurray. The thyristor electronic transformer: a power converter using a high-frequency link. *IEEE Transactions on Industry and General Applications*, IGA-7(4), July/August 1971.

[11] C. W. McLyman. *Transformer and Inductor Design Handbook*. CRC Press, 3 edition, 2004. ISBN 0824751159, 9780824751159.

[12] S. Khan, K. Rahman, M. Tariq, S. Hameed, B. Alamri, and T. S. Babu. Solid-state transformers: Fundamentals, topologies, applications, and future challenges. *Sustainability*, 14(1), 2022. ISSN 2071-1050. doi: 10.3390/su14010319.

[13] Y. Wang, O. Lucia, Z. Zhang, S. Gao, Y. Guan, and D. Xu. A review of high frequency power converters and related technologies. *IEEE Open Journal of the Industrial Electronics Society*, 1:247–260, 2020. doi: 10.1109/OJIES.2020.3023691.

[14] J. Biela, U. Badstuebner, and J. W. Kolar. Impact of power density maximization on efficiency of dc–dc converter systems. *IEEE Transactions on Power Electronics*, 24(1):288–300, 2009. doi: 10.1109/TPEL.2009.2006355.

[15] Z. Ouyang and M. A. E. Andersen. Overview of planar magnetic technology—fundamental properties. *IEEE Transactions on Power Electronics*, 29(9):4888–4900, 2014. doi: 10.1109/TPEL.2013.2283263.

[16] A. Ammouri, H. Belloumi, T. B. Salah, and F. Kourda. High-frequency investigation of planar transformers. In *2014 International Conference on Electrical Sciences and Technologies in Maghreb (CISTEM)*, pages 1–5, 2014. doi: 10.1109/CISTEM.2014.7076927.

[17] C. Quinn, K. Rinne, T. O'Donnell, M. Duffy, and C. Mathuna. A review of planar magnetic techniques and technologies. In *APEC 2001. Sixteenth Annual IEEE Applied Power Electronics Conference and Exposition (Cat. No.01CH37181)*, volume 2, pages 1175–1183 vol.2, 2001. doi: 10.1109/APEC.2001.912514.

[18] M. Bernardoni, N. Delmonte, P. Cova, and R. Menozzi. Thermal modeling of planar transformer for switching power converters. *Microelectronics Reliability*, 50:1778–1782, 09 2010. doi: 10.1016/j.microrel.2010.07.129.

[19] N. Dai, A. Lofti, C. Skutt, W. Tabisz, and F. Lee. A comparative study of high-frequency, low-profile planar transformer technologies. In *Proceedings of 1994 IEEE Applied Power Electronics Conference and Exposition - ASPEC'94*, pages 226–232 vol.1, 1994. doi: 10.1109/APEC.1994.316395.

[20] *2221: Generic Standard on Printed Board Design*. IPC Standards, 1998.

[21] N. Shahabi, F. Zare, A. Ghosh, and G. Ledwich. A new configuration for planar magnetic elements to reduce capacitive couplings. In *Proceedings of 14th International Power Electronics and Motion Control Conference EPE-PEMC 2010*, pages T6–126–T6–130, 2010. doi: 10.1109/EPEPEMC.2010.5606552.

[22] R. Pittini, Z. Zhang, Z. Ouyang, M. A. E. Andersen, and O. C. Thomsen. Analysis of planar e+i and er+i transformers for low-voltage high-current dc/dc converters with focus on winding losses and leakage inductance. In *Proceedings of The 7th International Power Electronics and Motion Control Conference*, volume 1, pages 488–493, 2012. doi: 10.1109/IPEMC.2012.6258778.

[23] C. Ropoteanu, P. Svasta, and C. Ionescu. Electro-thermal simulation study of different core shape planar transformer. In *2016 IEEE 22nd International Symposium for Design and Technology in Electronic Packaging (SIITME)*, pages 209–212, 2016. doi: 10.1109/SIITME.2016.7777279.

[24] S. Vaisambhayana, C. Dincan, C. Shuyu, A. Tripathi, T. Haonan, and B. R. Karthikeya. State of art survey for design of medium frequency high power transformer. In *2016 Asian Conference on Energy, Power and Transportation Electrification (ACEPT)*, pages 1–9, 2016. doi: 10.1109/ACEPT.2016.7811550.

[25] Z. Ouyang, O. C. Thomsen, and M. A. E. Andersen. Optimal design and tradeoff analysis of planar transformer in high-power dc–dc converters. *IEEE Transactions on Industrial Electronics*, 59(7):2800–2810, 2012. doi: 10.1109/TIE.2010.2046005.

[26] M. Nguyen and H. Blanchette. A review and comparison of solid, multi-strands and litz style pcb winding. *Electronics*, 9:1324, 08 2020. doi: 10.3390/electronics9081324.

[27] M. Nguyen and H. Blanchette. Optimizing ac resistance of solid pcb winding. *Electronics*, 9:875, 05 2020. doi: 10.3390/electronics9050875.

[28] *Ferrite Cores*. Magnetics Inc, . `https://www.mag-inc.com/Products/Ferrite-Cores`.

[29] *R Material*. Magnetics Inc, . `https://www.mag-inc.com/Products/Ferrite-Cores/R-Material`.

[30] *Ferrite Core Loss Calculator*. Magnetics Inc, . `https://www.mag-inc.com/Design/Design-Tools/Ferrite-Core-Loss-Calculator`.

[31] Z. Ouyang, O. C. Thomsen, and M. A. E. Andersen. The analysis and comparison of leakage inductance in different winding arrangements for planar transformer. In *2009 International Conference on Power Electronics and Drive Systems (PEDS)*, pages 1143–1148, 2009. doi: 10.1109/PEDS.2009.5385844.